

# FCM<sub>PASS</sub> Software Aids Extracellular Vesicle Light Scatter Standardization

Joshua A. Welsh,<sup>1,2\*</sup>  Peter Horak,<sup>3</sup>  James S. Wilkinson,<sup>3</sup>  Verity J. Ford,<sup>1</sup>  Jennifer C. Jones,<sup>2</sup>  David Smith,<sup>1,4</sup> Judith A. Holloway,<sup>1</sup>  Nicola A. Englyst<sup>1</sup> 

<sup>1</sup>Faculty of Medicine, University of Southampton, Southampton, UK

<sup>2</sup>Translational Nanobiology Section, Laboratory of Pathology, Center for Cancer Research, National Cancer Institute, National Institutes of Health, Bethesda, Maryland

<sup>3</sup>Optoelectronics Research Centre, University of Southampton, Southampton, UK

<sup>4</sup>Anaesthetics Department, University Hospital Southampton, Southampton UK

Received 14 December 2018; Revised 4 April 2019; Accepted 16 April 2019

Grant sponsor: European Association of Cardiothoracic Anaesthesiology; Grant sponsor: U.S. National Institutes of Health, National Cancer Institute, Grant number 1ZIA-BC011502; Grant sponsor: University of Southampton Higher Education Innovation Fund; Grant sponsor: University of Southampton, Faculty of Medicine, Doctoral Training Award scheme

Additional Supporting Information may be found in the online version of this article.

\*Correspondence to: Joshua A. Welsh, Translational Nanobiology Section, Laboratory of Pathology, Center for Cancer Research, National Cancer Institute, Building 10, Room B1B51, 10 Center Drive, NIH, Bethesda, Maryland, 20892, USA.  
Email: joshua.welsh@nih.gov

Published online in Wiley Online Library (wileyonlinelibrary.com)

DOI: 10.1002/cyto.a.23782

## Abstract

The study of extracellular vesicles (EVs) is a rapidly growing field due to their great potential in many areas of clinical medicine including diagnostics, prognostics, theranostics, and therapeutics. Flow cytometry is currently one of the most popular methods of analyzing EVs due to it being a high-throughput, multiparametric technique, that is readily available in the majority of research labs. Despite its wide use, few commercial flow cytometers are designed specifically for the detection of EVs. Many flow cytometers used for EV analysis are working at their detection limits and are unable to detect the majority of EVs. Currently, very little standardization exists for EV flow cytometry, which is an issue because flow cytometers vary considerably in the way they collect scattered or fluorescent light from particles being interrogated. This makes published research hard to interpret, compare, and in some cases, impossible to reproduce. Here we demonstrate a method of flow cytometer light scatter standardization, utilizing flow cytometer postacquisition analysis software (FCM<sub>PASS</sub>). FCM<sub>PASS</sub> is built upon Mie theory and enables the approximation of flow cytometer geometric parameters either by analyzing beads of known diameter and refractive index or by inputting the collection angle if known. The software is then able to create a scatter-diameter curve and scatter-refractive index curve that enables researchers to convert scattering data and instrument sensitivity into standardized units. Furthermore, with the correct controls, light scatter data can be converted to diameter distributions or refractive index distributions. FCM<sub>PASS</sub> therefore offers a freely available and ergonomic method of standardizing and further extending EV characterization using flow cytometry. Published 2019. This article is a U.S. Government work and is in the public domain in the USA. *Cytometry Part A* published by Wiley Periodicals, Inc. on behalf of International Society for Advancement of Cytometry.

## Key terms

extracellular vesicles; flow cytometry; standardization; light scatter; Mie modeling; software

**EXTRACELLULAR VESICLES** (EVs), which include exosomes (30–150 nm) and microvesicles (30–1,000 nm), are shed by cells, with other types also known to exist (1). These small vesicles have a phospholipid bilayer containing proteins and an inner cytosolic portion that contains cargo including proteins, metabolites, and/or genetic content (2,3). Research utilizing EVs is growing due to their diagnostic and therapeutic potential, with many laboratories opting to use flow cytometry for their detection (4). The full size range of EVs cannot be detected in the majority of conventional flow cytometers, which are developed to characterize cells.

Early literature using light scatter signals to gate EV populations employed reference particles such as polystyrene beads and, more recently, silica beads. For example, polystyrene reference beads of ~1 μm diameter have been used as reference particles for the larger diameter microvesicles (5–8). Polystyrene beads are also commonly used today by manufacturers to demonstrate flow cytometer scatter sensitivity. Using polystyrene or silica reference beads for EV sizing results in a systematic error in EV diameter

Published 2019. This article is a U.S. Government work and is in the public domain in the USA. *Cytometry Part A* published by Wiley Periodicals, Inc. on behalf of International Society for Advancement of Cytometry.

This is an open access article under the terms of the Creative Commons Attribution-NonCommercial License, which permits use, distribution and reproduction in any medium, provided the original work is properly cited and is not used for commercial purposes.

estimation, as the refractive indices of these beads differ significantly from that of EVs in their light scatter properties (9). A solution to this problem is converting the scatter parameter in arbitrary units to a standardized unit that would allow comparisons across cytometers. Developing a standardized unit for flow cytometer scatter is, however, nontrivial and must begin with basic models of Mie scattering and some basic concepts.

Light scatter is the process whereby light hits a particle and then changes direction, this includes reflection and refraction. In the context of flow cytometry, a laser beam is focused upon a stream in which particles are suspended. When a particle traverses through the laser beam, light is scattered in all directions by the illuminated particle. In conventional flow cytometry, light scatter is collected perpendicular to the illumination source, known as the parameter, side scatter (SSC), and in the same direction as the illumination source, known as the parameter, forward scatter (FSC). The amount of light scattered by a particle however is dependent on a large number of factors.

To quantify the amount of light reaching a detector in absolute units, the collection geometry of the system from the particle to the detector must be known, as this limits the photons that can reach the detector. The geometry that has the largest effect on the number of photons that reach the detector is the flow cell. Flow cells tend to be made of quartz and have inner and outer dimensions, both of which tend to be rectangles—although square flow cells are also used. The range of angles that can be collected by the SSC detector is most often limited by either the inner or the outer flow cell dimensions. Once the collection angle is known, calculating the collected light scatter from a particle can be carried out as there is now a range of angles to integrate the angular scattering distribution of the particle over.

Popular methodologies for determining the amount of light scattered from small particles are Mie scattering and Rayleigh scattering. Rayleigh scattering theory is the simpler methodology of the two, but only applies to predicting light scatter from particles whose diameter is less than one tenth of the incident wavelength. Mie scattering theory was first published in 1908 by Gustav Mie and is built upon the Maxwell equations, provides a means to calculate the angular light scattering distribution of spherical particles of any diameter, and has successfully been applied to flow cytometry (9,10). Furthermore, core-shell structures (Fig. 1B) such as EVs, which comprise of a cytosolic core and a membrane shell, can be readily modeled using Mie scattering. Mie scattering theory is therefore well-suited to modeling the scattering distribution of the full range of EVs as well as homogeneous spheres (Fig. 1C) of polystyrene and silica reference beads.

While mathematically it is possible to predict the power of collected light scatter from a particle, collected within a certain geometry, there are several variables to account for which are hard to measure, including: the transmission efficiency of light from the particle to the detector, the laser intensity, and detector variables such as quantum efficiency, as well as user-defined detector variable such as gain and voltage. Normalizing flow cytometry light scatter data from arbitrary units to standard units of scattering in power is therefore difficult. We believe the most practical unit to normalize the arbitrary scattering measurements is the scattering cross section; this is obtained by integrating the differential scattering cross section over the angles collected by the detector within the flow cytometer. The scattering cross section is a hypothetical area describing the probability of light, with unit incident irradiance, being scattered by a particle. The power of scattered light is directly proportional to this cross section and to the incident laser power. The calculation of integrated scattering cross section however requires fewer instrument variables to be measured for its calculation. For small particles, the scattering cross sections is best denoted in units of  $\text{nm}^2$ . From here on in we refer to the scattering cross section as the collected light integrated over the collection range of the system.

In this article, we give an illustration of the interdependence of collection angle, diameter, and refractive index using Mie theory. We then go on to demonstrate the ability of the FCM<sub>PASS</sub> software to (1) experimentally estimate the half-angle of the collection cone for three commercial flow cytometers, (2) show that approximating the cytometer collection angle can lead to accurate sizing of a range of NIST-traceable beads in various instruments and (3) apply standardized units to flow cytometry SSC data.

## METHODS

### Modeling of Light Scattering by Nanoparticles

To predict the angular light scattering behavior of particles, a numerical model for scattering from coated and homogeneous spheres from a linearly polarized incident plane wave was implemented in MATLAB (v. 9.0.0.341360, Mathworks, Inc., Natick, MA), based on Mie theory, using the scripts by C. Maetzler and the formalism of Bohren and Huffman (11,12). These calculations are similar to those previously reported (9,13,14). The scattering cross sections plotted are based on the sum of intensities of the two orthogonal components,  $S_1^2$  and  $S_2^2$ . Further details of the calculation can be found in Supporting Information 1. The coated spheres modeled are based on the membrane and cytosol of EVs with refractive indices taken from the literature (13,15–19), while the homogenous spheres modeled are based on the reference

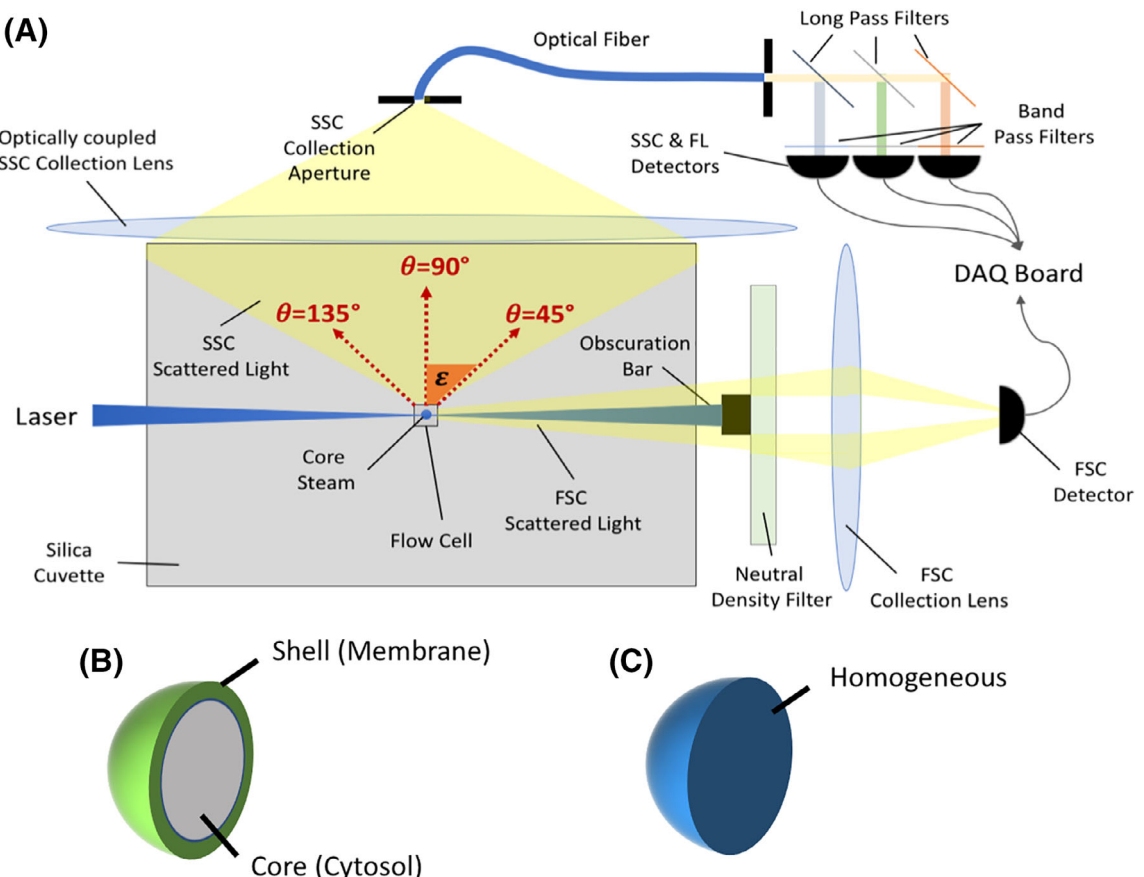


**Figure 1.** Top view schematic of a flow cytometer with optical fiber and particle composition. **(A)** Particles confined in the core stream (propagating out of the image plane) scatter light from the laser; the direction of scattered light is given by the angle  $\theta$ . The SSC optics collects the scattered light within the collection half-angle  $\epsilon$  symmetrically at directions perpendicular to the laser propagation direction, that is, light is collected from scattering directions  $\theta$  between  $90^\circ - \epsilon$  and  $90^\circ + \epsilon$ . It can be seen that in this case the outer flow cell is the limiting collection angle, which is common. However, any component in the path between the illuminated particle and the light received by the detector can alter the collection angle and geometry of the system. **(B)** Core-shell structure representing how an extracellular vesicle would be modeled. The shell representing the phospholipid bilayer, typically 10 nm, and the core representing the cytosolic portion. **(C)** Homogeneous sphere representing how silica and polystyrene beads are modeled.

particles with refractive indices given by the Sellmeier Equations (20) for silica:

$$n^2 - 1 = \frac{0.6961663\lambda^2}{0.0684043^2} + \frac{0.4079426^2}{\lambda^2 - 0.1162414^2} + \frac{0.897494\lambda^2}{\lambda^2 - 9.896161^2}$$

and polystyrene:

$$n^2 - 1 = \frac{1.4435\lambda^2}{\lambda^2 - 0.020216}$$

The particle diameters modeled ranged from 1 to 3,000 nm to cover both EVs and reference particles (9). Angular scattering distributions for  $\theta$  were determined in  $1^\circ$  increments from  $0^\circ$  to  $180^\circ$  in relation to the incident beam, for each modeled particle. Models showing the angular scattering distribution were not integrated over  $\phi$ . Scattering cross sections for flow cytometer models were calculated by using flow cytometer collection angles as an integral over the

differential scattering cross section. The collection angles assumed symmetrical collection at  $90^\circ$  to the incident laser beam, in order to model the collection of side-scattered light through a finite aperture. See Figure 1A for a schematic of the geometry, see Supporting Information for further details on Mie calculations.

#### Analysis of Beads by Flow Cytometry

NIST-traceable beads, Table 1, were serially diluted in Dulbecco's phosphate-buffered saline until a concentration minimizing coincidence detection with a stable light scatter intensity was determined. Beads were analyzed at the lowest flow rate obtainable on each instrument and a minimum of 5,000 events were recorded. Flow cytometer voltages were adjusted so that the beads with the maximum and minimum scattering were within the dynamic range of the side scattering collection (SSC) detector. Thresholds were set on SSC on all instruments and were placed so that they were below the 203 and 490 nm bead populations. Instruments used were

## TECHNICAL NOTE

**Table 1.** Manufacturer specifications of the NIST bead diameters used in the experiment and for modeling

| COMPOSITION | DIAMETER (NM $\pm$ SD) | REFRACTIVE INDEX (AT 589 NM) |
|-------------|------------------------|------------------------------|
| Polystyrene | 203 $\pm$ 5            | 1.59                         |
|             | 400 $\pm$ 7            | 1.59                         |
|             | 707 $\pm$ 8            | 1.59                         |
|             | 1,019 $\pm$ 10         | 1.59                         |
|             | 1,587 $\pm$ 21         | 1.59                         |
| Silica      | 490 $\pm$ 20           | 1.45                         |
|             | 730 $\pm$ 30           | 1.45                         |
|             | 990 $\pm$ 20           | 1.46                         |
|             | 1,570 $\pm$ 40         | 1.46                         |

LSR Fortessa, FACS Canto I, and Special Order LSR Fortessa X-20 (all by Becton Dickinson, Oxford, UK). All flow cytometers used an optical bandpass filter centered at 488 nm wavelength with a bandwidth of 10 nm (488/10 filter).

### Flow Cytometer Calibration with Reference Particles and Particle Diameter Estimation

Acquired bead data from each cytometer was inputted into postanalysis software, FlowJo v10.1 (FlowJo LLC, Ashland). Each bead population was gated individually with the SSC statistics calculated for each. This SSC statistics for each population were then inputted into a MATLAB script that also contained the bead population mean diameter and refractive index from the manufacturer's technical specifications, Table 1.

Once the instrument SSC collection angle was determined (either by considering the imaging optics or by fitting the simulations to the measured data, see Results section), this angle was then used to create predicted data for the beads, creating a curve for each unique bead refractive index. Recorded SSC values from each of the instruments were normalized to their predicted data with a single normalization factor, in order to relate the arbitrary flow cytometer channel count units to the particle scattering cross section in absolute units of nm<sup>2</sup> as calculated by the MATLAB scripts using Mie theory. This single normalization factor was obtained as the mean of the normalization factors of each bead population, calculated by dividing the measured SSC value by the predicted value for each population. These scripts were compiled into the publicly available "FCM<sub>PASS</sub>", available at <https://go.cancer.gov/a/y4ZeFtA>. Supporting Information Table 1 shows the development of the software.

### Biological Sample Preparation & Analysis

Blood samples were taken from a biobank of patients undergoing cardiac bypass surgery. Ethics approval was given by the South Central NRES committee (Ref: 11/SC/0214) and the University of Southampton ERGO committee (Submission ID:14646). The participant provided written informed consent. All sample and participant data were link anonymised, with the master key kept under secure storage. Samples were acquired from the port of the central venous line. The first 3 ml of blood was discarded before

collecting the 6 ml sample into lithium heparin-coated Vacutainer tubes (BD Biosciences, Oxford, UK). Shear-stress was minimized by breaking the Vacutainer seal before sample collection. Samples were centrifuged within 1 h twice at 2000 RCF for 10 min at room temperature, isolating platelet poor plasma (PPP). The sample was initially stored at -20°C until transportation to -80°C freezers. The PPP sample was thawed at 37°C for 10 min before 30 µl of PPP was added to 50 µl 0.1 µm double-filtered HEPES buffered saline (dfHBS) with 3 µl of 200 µg mL<sup>-1</sup> anti-human CD41a IgG1κ BV421 (Cat. 624124, Lot. 4231719, BD Bioscience, Oxford, UK). Samples were incubated for 5 min before 10 µl of 83 µg mL<sup>-1</sup> MGEG8 FITC (Cat. BLAC-FITC, Lot. EE0318-1ML, Cambridge Bioscience, Cambridge, UK) was added and incubated on ice in the dark for a further 10 min before analysis using flow cytometry. Following incubation, 1 ml of 0.1 µm dfHBS was added to the incubated sample. Samples were serially diluted to find a concentration that reduced the likelihood of simultaneous detection of two or more particles in the illuminated part of the core stream at once. When an appropriate dilution factor for the sample was determined, the sample was then analyzed in a tube containing 1 ml 0.1 µm dfHBS and a known number of fluorescent counting beads for enumeration of the sample volume (TruCount Tubes, BD Bioscience, Oxford, UK). An isotype matched control (mouse IgG1κ BV421, Cat. 562438 Lot. 4115857, BD Bioscience, Oxford, UK) was used at the same final concentration as the anti-human CD41a antibody, and analyzed at the same dilution as their matched antibody sample. Detailed information on experiment design and acquisition for EVs can be found in Supporting Information Table 2.

## RESULTS

### Interdependence of Collection Angle, Diameter, and RI on Small Particle Scattering Using Mie Theory

**Diameter and composition.** In later sections of this work, we will discuss how to calibrate commercial flow cytometers using reference beads made of known materials: silica and polystyrene, and with known diameters. We thus start with a brief review of how light is scattered by homogeneous nanospheres and compare this with scattering by EVs, modeled as homogenous spheres covered by a thin membrane of higher refractive index. The discussions are based on Mie theory (see Methods section for more details).

The total scattering cross section is obtained from the differential cross section by integration over all solid angles. In the majority of commercial flow cytometers, SSC is collected at 90° to the illumination source. Due to the varying geometries of the collection optics the half-angle (shown as 'e' in Fig. 1A) varies. This angle can also vary due to alignment by service engineers and may in part explain the variability that can be seen between the same instruments. This can have a large impact in the comparability between flow cytometers with large differences in collection half-angle due to the nonlinear nature of particle scattering. Figure 2 shows the differential scattering cross section as a function of the direction

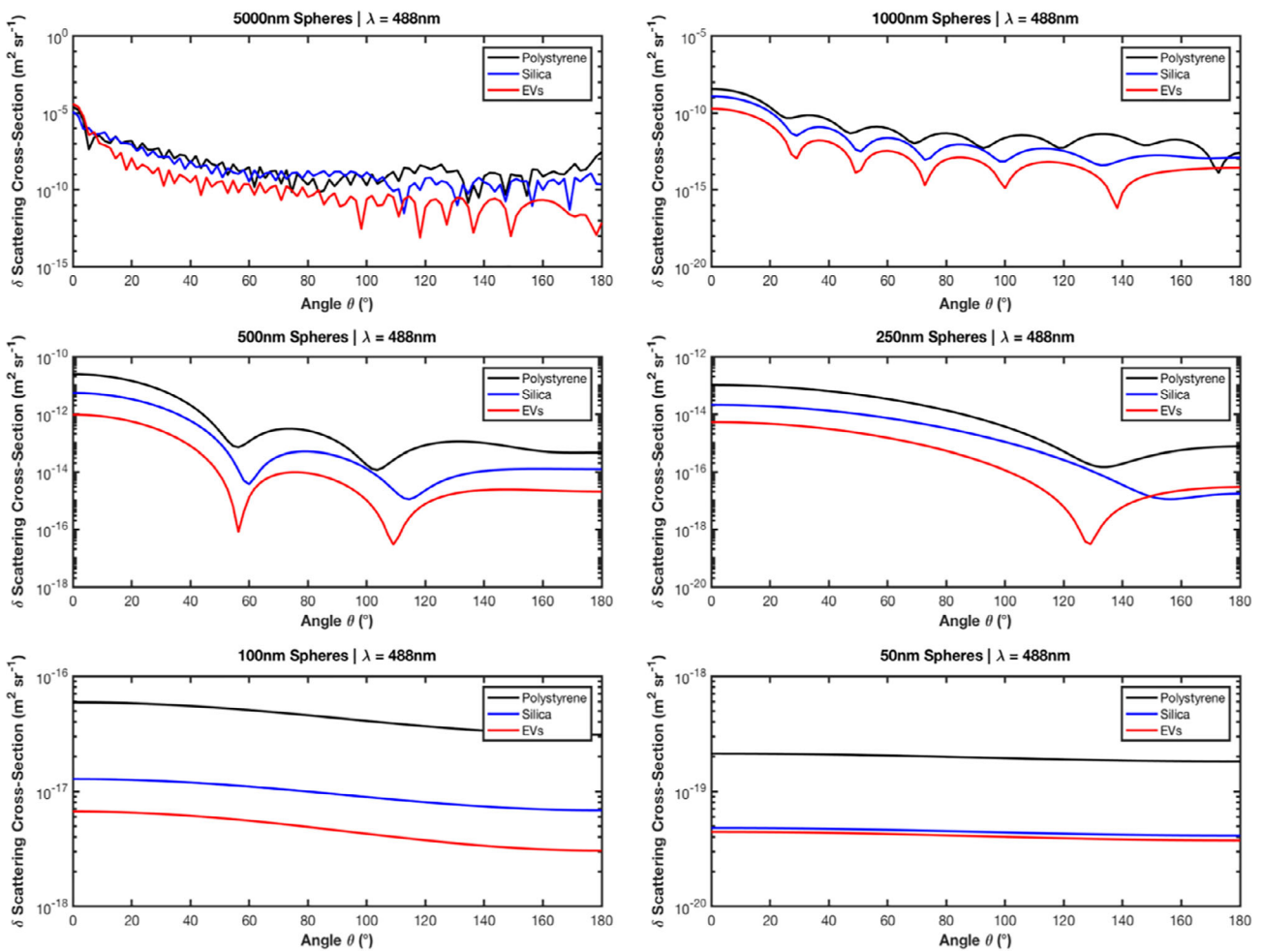


**Figure 2.** Effect of diameter and composition on angular scattering distribution. Angle-dependence of light scattering differential cross section for microparticles of different composition and different diameters calculated by Mie scattering theory for illumination at 488 nm wavelength. Polystyrene and silica beads are modeled as homogeneous spheres, vesicles as spheres with different refractive indices for the cytosol and for a 10 nm thick membrane.

of the scattered light (angle  $\epsilon$  in Fig. 1A) for polystyrene and silica beads and EVs of different diameters for illumination at 488 nm wavelength, whose physical properties are given in Table 2.

The first thing of note from Figure 2 are the series of peaks and troughs, known as Mie resonances. There are more Mie resonances in larger particles than smaller particles, this is because they are largely dependent on the ratio of the particle's diameter to the illumination wavelength. Second, the position of the Mie resonances is not consistent. It can be seen that particles with the same diameter but different refractive indices have Mie resonances that appear at different angles. Third, the lower the refractive index, the less cumulative light is scattered by the particle and the deeper the Mie resonances tend to be.

These three factors are important for when we consider a flow cytometer's optics, which collects the sum of light over a range of angles. Many modern flow cytometry analysers have a SSC collection half-angle ( $\epsilon$ )  $\sim 50^\circ$ . In the case of Figure 2,

it would mean the collected light of each of the particles would be the sum of all angles from  $40^\circ$  to  $140^\circ$ . Jet-in-air sorters however tend to have a collection half-angle of  $\sim 30^\circ$ , meaning the collected light would be the sum of angles from  $60^\circ$  to  $120^\circ$ . If these two collections angles are considered for 250 nm particles in Figure 2, it would mean that the deep Mie resonance by the EV composition at  $130^\circ$  would be fully collected by a generic

**Table 2.** Refractive indices of materials used within flow cytometer modeling

| MATERIAL    | REFRACTIVE INDEX AT WAVELENGTH |        |        |
|-------------|--------------------------------|--------|--------|
|             | 405 NM                         | 488 NM | 633 NM |
| Water       | 1.345                          | 1.337  | 1.334  |
| Polystyrene | 1.624                          | 1.604  | 1.586  |
| Silica      | 1.470                          | 1.463  | 1.457  |
| EV Membrane | NA                             | 1.480  | NA     |
| EV Cytosol  | NA                             | 1.380  | NA     |

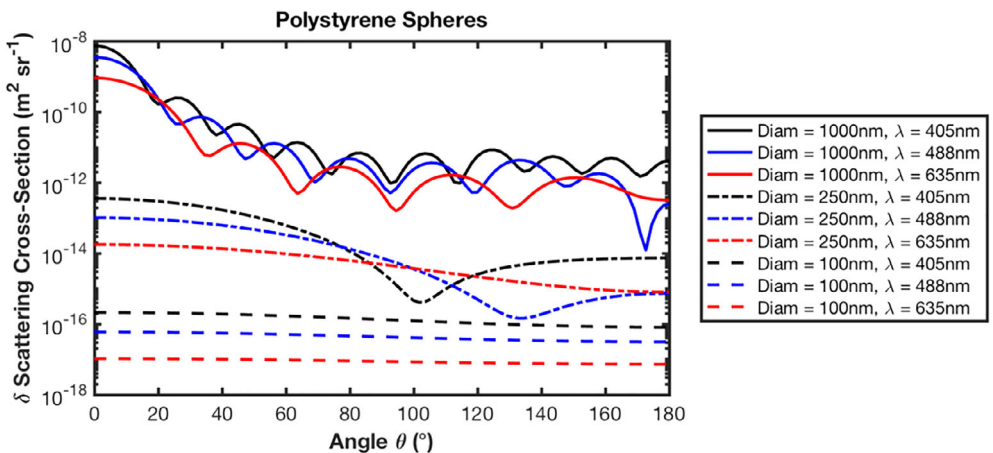


**Figure 3.** Effect of wavelength of angular scattering distribution. Angle-dependence of light scattering differential cross section for silica beads of different diameters at different illumination wavelengths calculated by Mie scattering theory. Bead diameters are 5,000 nm (solid lines), 500 nm (dashed), 100 nm (dotted), and light wavelengths are 405 nm (blue lines), 488 nm (green), 633 nm (red).

analyzer, which collects light up to  $140^\circ$  but not by a generic jet-in-air sorter, which would collect light up to  $120^\circ$ . The ratio of the EV collected light would therefore be different to that of the beads between the cytometers.

Overall there is no simple relationship between the scattered light intensities in a given direction for different particles since the Mie resonances also shift with the particle refractive index.

**Illumination wavelength.** While scattered light tends to be collected at 488 nm wavelength in conventional flow cytometers, it is possible to collect light scatter at different wavelengths in multilaser configured flow cytometers, with some new generation flow cytometers choosing to collect light at 405 nm. As an example, we thus show a selection of differential scattering cross sections for silica spheres at three different wavelengths in Figure 3 (The effect of wavelength, from 405 to 640 nm, on polystyrene and silica bead scattering can be seen in the video of Supporting Information Video 1). While generally similar behavior to Figure 2 is found here, we note that the exact details of light scattering, such as absolute values of cross sections and positions of Mie resonances, depend significantly on the illumination wavelength due to the wavelength dependence of refractive indices as well as the differing ratio of light wavelength compared to particle size, as mentioned above.

The data shown in Figures 2 and Figure 3 demonstrate that the particle angular scattering distribution varies with both size and composition; therefore, the diameter of a particle cannot be inferred unless its refractive index and the angle of light collection in the flow cytometer are known.

The illumination beam polarization is also a critical factor when calculating these models and can lead to large inaccuracies if not accounted for, particularly when small collection half-angles are involved. Most flow cytometer illumination beams are linearly polarized, all presented models therefore make this assumption. While illumination beam polarization is

important to account for, demonstrating the effects of illumination beam polarization on particle angular light scattering distributions is beyond the scope of this work.

### Collection Angle

When particles are suspended in a flow stream and passed through a laser beam in a flow cytometer, only a portion of their scattered light is collected. Flow cytometers typically collect light in the forward direction and in the sideward direction. Many flow cytometers have a higher sensitivity to small particles using side scatter, rather than forward scatter detection, and SSC has therefore mainly been used to gate EVs based on size. This is because side scatter generally allows wider collection angles and because it is well separated from the forward propagating laser beam.

In conventional flow cytometer, SSC is most commonly collected from a cone of half-angle  $\epsilon$  at a perpendicular angle to the illuminating laser beam as shown in Figure 1A and this is the case in all flow cytometers described in this article. The maximum range of collection angles of a particle's light scatter is determined by a number of parameters, most notably the flow cell geometry, cuvette geometry, lens numerical aperture and alignment, but may also be affected by the central focusing and diameter of the core stream, the suspending medium refractive index, and other details of the collection optics.

Consequently, the amount of light collected by SSC in a flow cytometer corresponds to the differential scattering cross section (as shown in Fig. 2) integrated over a certain range of angles around  $90^\circ$ . This integrated cross section as a function of particle composition and size is shown in Figure 4 for different opening half angles of the collection optics ( $\epsilon$  from  $0^\circ$  to  $90^\circ$ ). This comparison is also shown for two optical geometries: "circular aperture" where light emitted in a cone of the given collection angle is collected, and "square aperture" where light emitted within the collection angle in both the azimuthal and polar angle is collected, Supporting Information Figure 2.

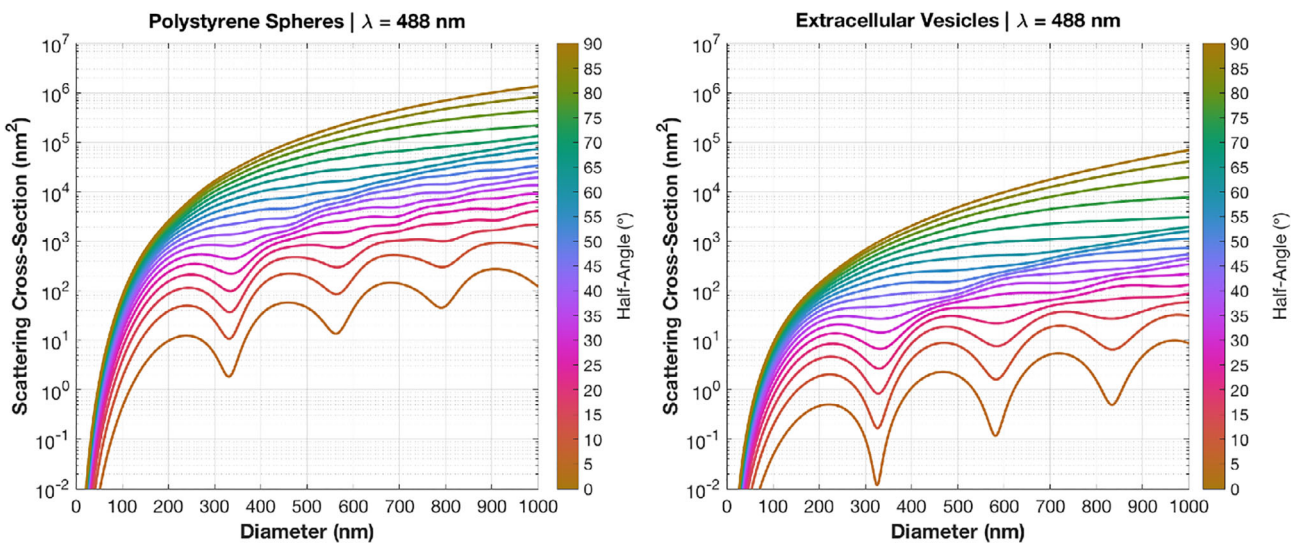


**Figure 4.** Effect of collection angle on scatter-diameter curves. Scattering cross sections integrated over finite collection half angles  $\varepsilon$  from 5° to 90° in 5° increments with circular apertures for polystyrene spheres (left) and extracellular vesicles (right) versus particle diameter, obtained from integration of the data in Figure 1 over the corresponding solid angles.

When all angles are collected between 0 and 180°, that is, for a collection half angle  $\varepsilon = 90^\circ$ , the integrated scattering cross section increases continuously with the particle diameter. As the collection angle decreases, the effect of Mie resonances becomes increasingly pronounced. For small collection half-angles, it is therefore no longer possible to uniquely determine a particle's diameter from a single light scatter detector. Both circular and square aperture geometries exhibit very similar behaviour with only very subtle differences (Supporting Information Fig. 2).

#### Calibration of Flow Cytometers Using FCM<sub>PASS</sub> Software

Based on the discussions above, it is therefore clear that in order to derive reliable estimates of EV diameters using conventional flow cytometry one needs to know the collection angle  $\varepsilon$  of the instrument. One obvious method to obtain the collection angle is by analyzing the imaging optics of the flow cytometer (9). However, gaining access to proprietary flow cytometer information may not be possible for many laboratories. As an alternative method, we show that the FCM<sub>PASS</sub> software can obtain a collection half-angle by numerically fitting measured SSC data for known reference particles with simulation results. We performed this analysis for three different flow cytometers: LSR Fortessa, LSR Fortessa X-20, and FACSCanto I.

First, we used analyzed polystyrene and silica NIST-traceable beads of different diameters, Table 1, to measure their SSC intensities. The median SSC peak height intensities for each bead were inputted into the software. Upon finishing its calculations, the FCM<sub>PASS</sub> software outputs 4 graphs Figure 5A-D. The FCM<sub>PASS</sub> software first calculates the approximate collection angle by comparing the acquired bead data with every possible collection half-angle from 0° to 90° in 0.1° increments, Figure 5A. The approximated collection angles

for each of the cytometers the calibration was performed upon produced results accurate to within 3° (Table 3). Upon approximating the collection half-angle, the predicted scattering cross section of the each of the beads is plotted against the acquired scattering intensity with linear regression then performed, Figure 5B. The obtained regression equation allows the conversion of SSC data in arbitrary units to units of scattering cross section in nm<sup>2</sup>. With this information, the software plots a scatter-diameter graph, Figure 5C, that allows the diameter versus intensity relationship to be observed irrespective of refractive index. The final graph is the scatter-refractive index plot, which plots the refractive index versus intensity relationship irrespective of diameter. Figure 5C, D can both be used to interpolate acquired scattering data with modeled scattering data to produce diameter distributions or refractive index distributions.

The manufacturer-specified diameter distributions and refractive index distributions of the acquired beads can be seen in Figure 6A, B. The acquired data from the beads in Figure 5 were interpolated with Figure 5C to produce the calculated diameter distributions of each bead in Figure 6C, and also interpolated with Figure 5D to produce the calculated refractive index distributions of each bead in Figure 6D. This was repeated for each cytometer with the comparisons summarized in Figure 7A,B. A more recent demonstration using a CytoFlex was carried out with different-sized NIST-Traceable polystyrene and silica beads, Supporting Information Figure 3.

To perform an interpolation of acquired scattering data to output refractive index distributions, the particles diameter must be known. Acquiring an accurate diameter distribution for EVs must be done with an independent measurement of the sample. This measurement can then be correlated with membrane intensity staining as previously demonstrated, assuming the cytometer used is able to resolve the total

## TECHNICAL NOTE

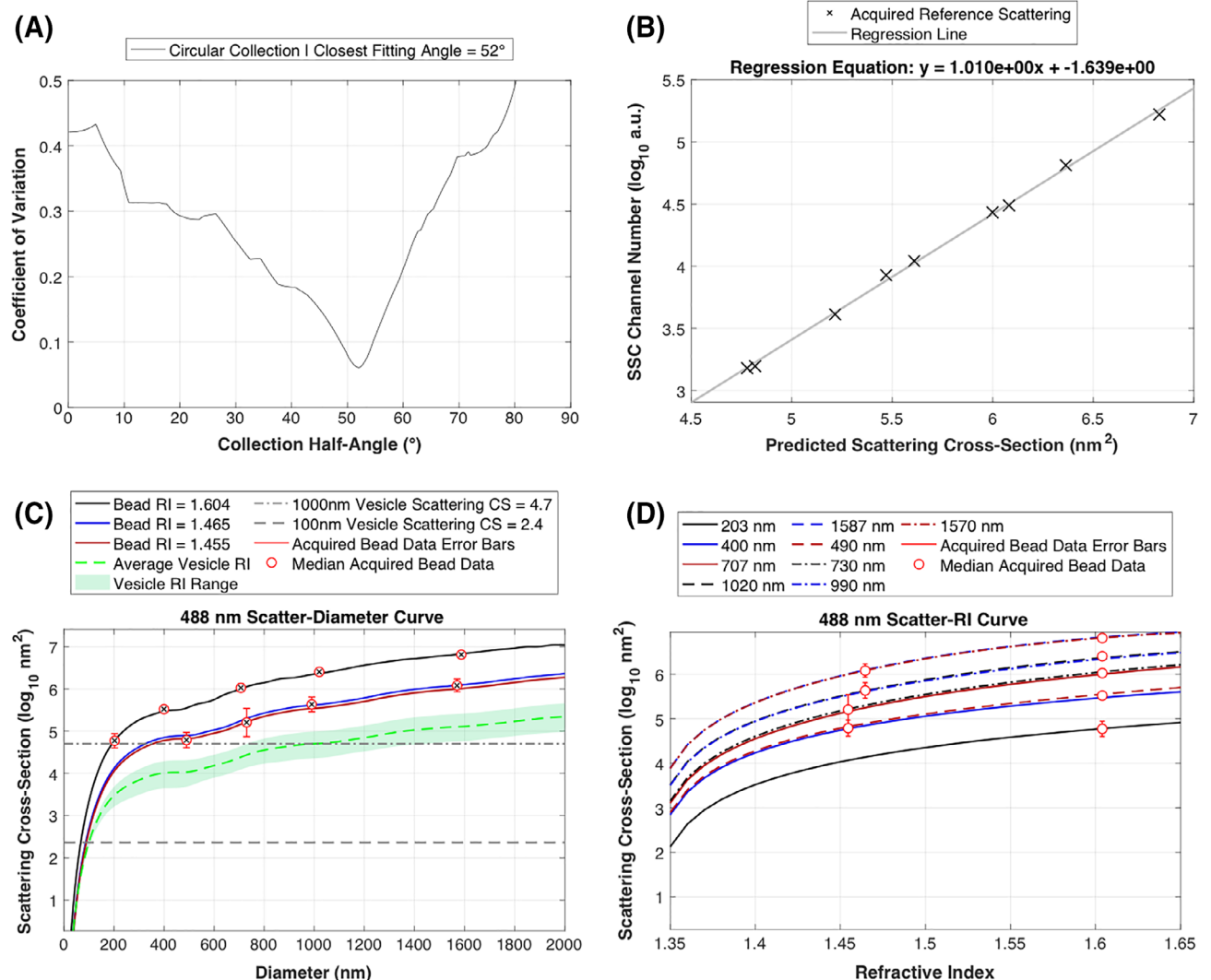


**Figure 5.** FCM<sub>PASS</sub> output figures from Fortessa X-20 analysis. (A) shows the coefficient of variation (CV) between predicted versus acquired scattering data from NIST-traceable beads. The collection half-angle with the lowest CV is deemed the collection half-angle for the instrument. (B) shows a linear regression of predicted versus acquired data for each bead, with the regression equation providing a means to convert arbitrary scattering data to known units of scattering cross-section in  $\text{nm}^2$ . (C) shows the median SSC-H versus diameter of each bead overlaid with the predicted scattering data for each NIST-traceable bead composition. (D) shows the median SSC-H versus refractive index of each NIST-traceable bead overlaid with the predicted scattering data for each bead composition.

membrane-stained population (21). To obtain a diameter distribution using interpolation with the scattering data, a refractive index must be assumed. While limited, EV refractive index determination has been demonstrated using NTA or using refractive index data based upon published measurements (13,15–19). It is therefore possible to generate an approximate refractive index using a core-shell model with upper and lower limits. While this is an approximation, current EV refractive index measurements fit within these bounds. Furthermore, provided the results of the interpolation are reported correctly, it is always possible to reproduce or revise the interpolated data when more accurate information becomes available.

With the flow cytometer calibration procedure described above, it is theoretically possible to approximate the

diameters of EVs with a known refractive index, as was demonstrated with beads of known refractive index. It should be noted that using this method to approximate the EV diameter distribution should be applied to a population that will not be positive for other particles such as lipoproteins, protein complexes, and so forth. Figure 8 demonstrates how diameter distribution can be approximated from scattering data, assuming an average EV refractive index. PPP was stained and gated around anti-CD41 and MFG-E8 staining. The fluorescently positive gated data Figure 8A was then interpolated with a scatter-diameter curve such as Figure 5C, to produce an approximate EV diameter distribution Figure 8C. The resulting diameter distributions fall within each detector bin in a nonlinear manner as a result of the multimodal Mie curves. Thus, the interpolated diameter

**Table 3.** Collection angle for side scattered light for several commercial flow cytometers. The “geometric angle” is obtained from the actual geometry of the imaging optics in the instruments, the “fitted angle” is the one obtained by fitting measured scattered intensities of test particles with our numerical model

|                   | COLLECTION HALF-ANGLE (°) |              |            |
|-------------------|---------------------------|--------------|------------|
|                   | GEOMETRIC ANGLE           | FITTED ANGLE | DIFFERENCE |
| LSR Fortessa X-20 | 52                        | 52.05        | 0.05       |
| LSR Fortessa      | 52                        | 49.65        | 2.35       |
| FACS Canto I      | 52                        | 54.60        | 2.60       |

distribution is a function of several instrument-specific attributes, including collection angles, light scattering geometries, channel binning, and signal processing algorithms.

Comparisons of phosphatidylserine staining using MFGE8 to 100 nm fluorescent beads and performance test beads can be seen in Supporting Information Figure 4. It can be seen that the diameter distribution appears to be bi-modal (Fig. 8C), with a trough in the range of ~400–480 nm. This trough is an artifact that results from the transposition of the arbitrary light scatter units to diameter (nanometers). This is a direct result of the flow cytometer collection angle and geometry and can be seen in Figure 8C where there is a plateau in the scatter-diameter curve from ~400 to 480 nm for the predicted EV light scattering using an average EV RI.

To further explain the effect of this type of artifact, a data set was created that had 1 event per detector channel from 200 to  $2^{18}$  (the maximum channel number in the Fortessa X-20), Supporting Information Figure 5. Interpolating this data set with the predicted data for the plotted

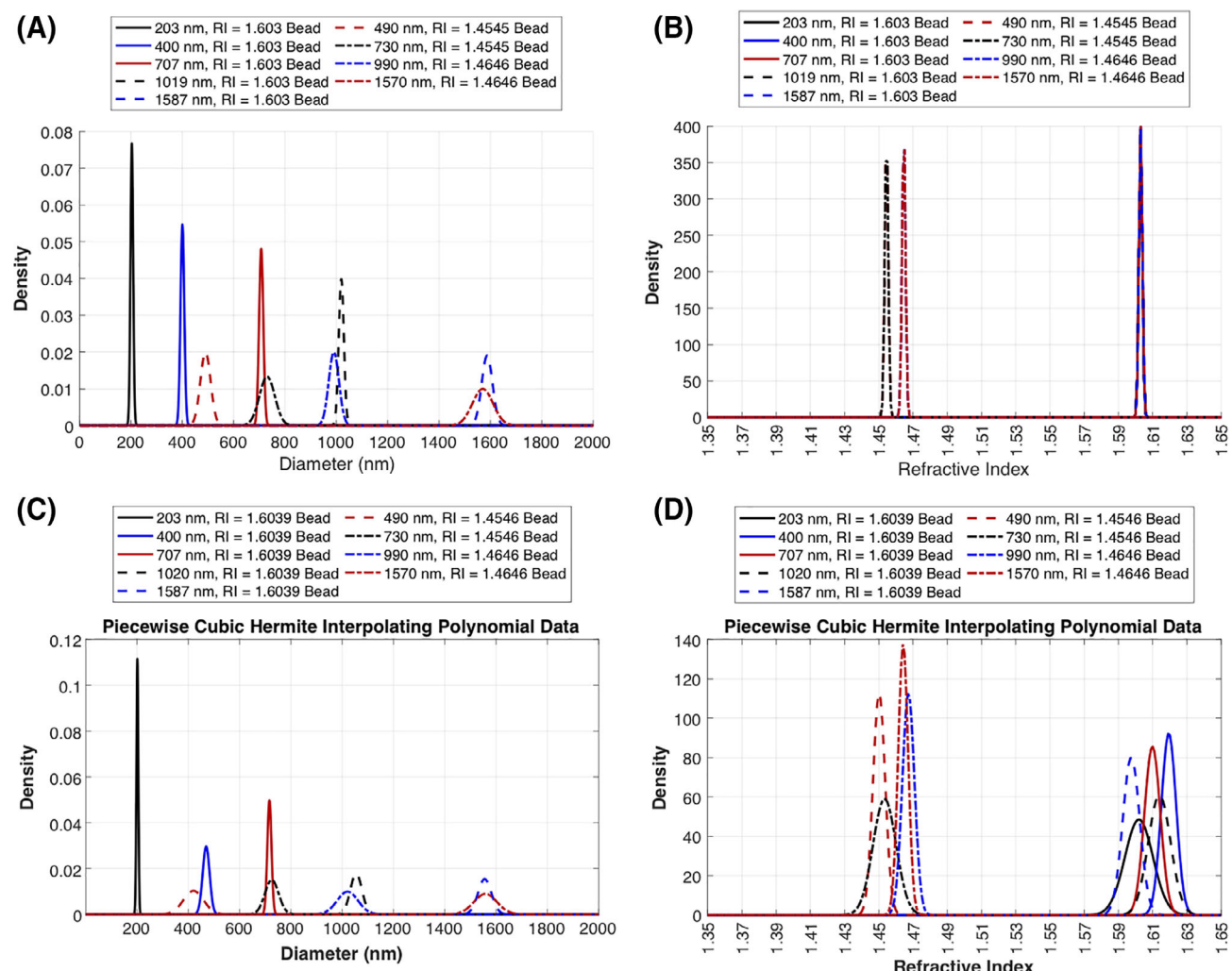


**Figure 6.** FCM<sub>PASS</sub> NIST-traceable bead interpolation from Fortessa X-20 analysis. (A) shows the expected mean bead diameter and coefficient of variation (CV) of each NIST-traceable bead, based on manufacturer specifications. (B) shows the expected refractive index and CV of each NIST-traceable bead, based on manufacturer specifications. (C) shows the obtained mean bead diameter and CV of each NIST-traceable bead, based on piecewise cubic hermite polynomial interpolation with modeled data. (D) shows the obtained mean bead RI and CV of each NIST-traceable bead, based on piecewise cubic hermite polynomial interpolation with modeled data.

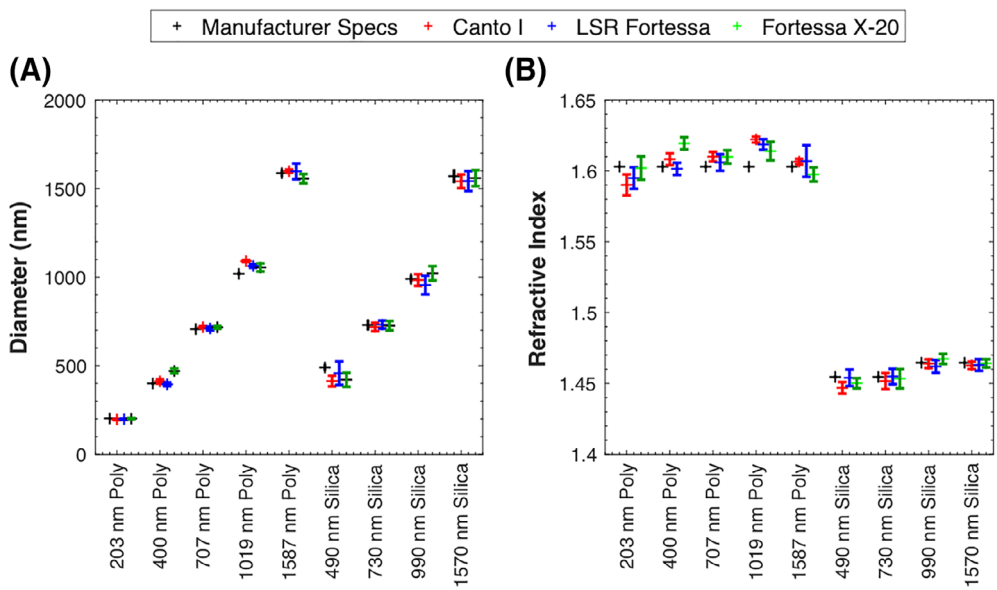


**Figure 7.** FCM<sub>PASS</sub> NIST-traceable bead interpolation cytometer comparison. (A) shows a comparison between expected (black) mean bead diameter and standard deviation (SD) of each NIST-traceable bead based on manufacturers specifications, and obtained mean bead diameter and SD from three different cytometers based on piecewise cubic hermite polynomial interpolation with modeled data. (B) shows a comparison between expected (black) mean refractive index and SD of each NIST-traceable bead based on manufacturers specifications, and obtained mean refractive index and SD from three different cytometers based on piecewise cubic hermite polynomial interpolation with modeled data.

average EV RI curve shows the resulting diameter distribution, where there is again a trough between ~400 and 480 nm. This artifact further highlights the importance of understanding the flow cytometer collection optics with regard to scattering for its standardization across instruments.

## DISCUSSION

This data demonstrates the relationship of particle scattering with composition, diameter, and illumination wavelength. We have also demonstrated that the FCM<sub>PASS</sub> software is capable of calibrating a flow cytometer's SSC parameter to produce standardized scattering measurements, by using numerical modeling of particle light scattering characteristics combined with reference particles. Importantly, utilizing this technique requires only the acquisition of commercial nanoparticles, with known diameter and refractive index, without the need to acquire proprietary or unknown flow cytometer information. Options are however available for users to specify set collection angles and geometries for modeling. It should be noted that the FCM<sub>PASS</sub> software, and modeling in general, is most reliable in flow cell-based flow cytometers. Flow cytometers, such as "jet-in-air" sorters have a user calibrated stream position, with respect to the collection optics, along with having SSC obscuration bars (22). Extra care with jet-in-air flow cytometer calibration and further calculations must therefore be carried to ensure the accuracy of SSC modeling, but it is feasible (23–25).

Furthermore, the FCM<sub>PASS</sub> software opens up avenues to allow the conversion of scattering intensity in arbitrary units to either a refractive index measurement or diameter distribution, provided the correct controls are performed. Utilization of the

FCM<sub>PASS</sub> software in the EV field could therefore be extremely beneficial in standardization of SSC data reporting and also allowing diameter or refractive index measurements between EV sources. While there are limitations in the transposing of arbitrary scattering units to diameters, due to the certain collection angles, as demonstrated within this manuscript, they tend to apply larger vesicles and in highly sensitive systems will account for minority of vesicles, due to the diameter distribution of EVs being a power law distribution (26).

In order to successfully use this technique in different laboratories, it is important to understand that this technique is reliant on an adequate number of nanoparticle diameters and refractive indices being used, with the reliability of approximated collection angle increasing with a larger number of bead diameters and compositions analyzed. We recommend at least eight bead diameters that are used with at least two compositions to allow for accurate calibration. This methodology for predicting collection angle is currently limited to conventional flow cytometer SSC collection optics, which are collected symmetrically and perpendicular to their illumination. Flow cytometers, such as the Apogee series of instruments, that collect light asymmetrically will still be able to calibrate their measurements using the software but users will have to input the collection angles manually.

Understanding the implications of EV scattering characteristics has an impact on the interpretation of current EV literature. First, it can clearly be seen that high refractive index materials, such as polystyrene, can only be related to EVs using light scattering if they are calibrated using modeling, for example, by Mie theory. A method for comparing what a flow cytometer is capable of detecting using light scatter and

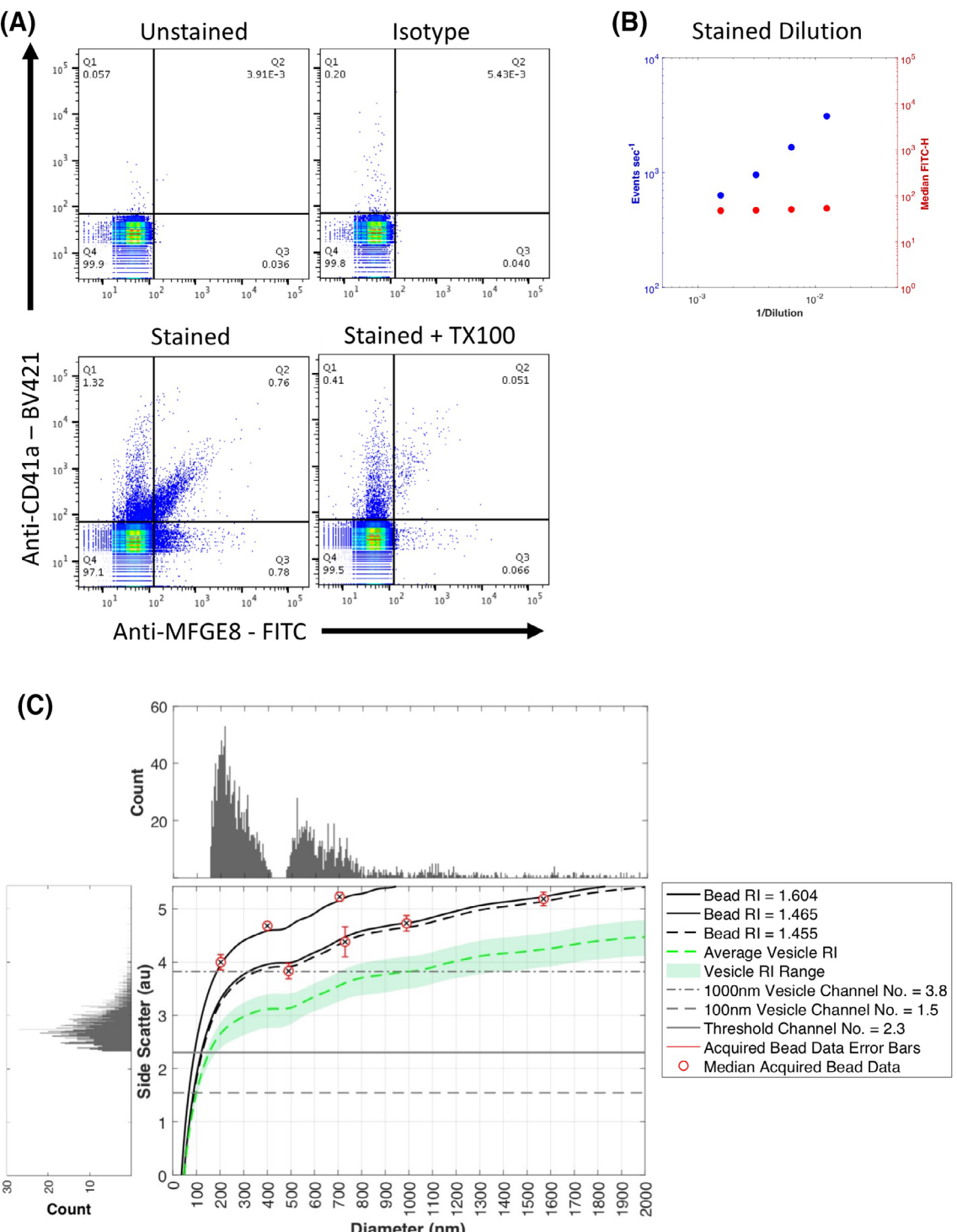


**Figure 8.** Analyzed platelet EVs. **(A)** shows dot plots for unstained, isotype, stained, and stained + triton X-100 EV populations. **(B)** shows dilution controls of EVs, **(C)** shows the CD41a + MFGE8+ EVs SSC histogram (left) plotted against the Fortessa X-20 scatter-diameter curve, used to interpolate the SSC data with the average EV RI plotted line to create a diameter distribution (top).

that does not use modeling would require a well-characterized reproducible control that mimics the scatter characteristics of EVs. This type of solution would not provide a way to calibrate axis to standard units or determine the limit of light scatter sensitivity without utilizing light scatter modeling. A

need for EV mimetics has been recognized within the field and is under investigation (17,27). A method that uses the ratio of forward scatter to side scatter without modeling has been demonstrated to derive particle refractive index, this methodology however is limited by the forward scatter

## TECHNICAL NOTE

sensitivity and will likely never be capable of utilization for the majority of EVs, which lie in the 100 nm EV diameter range. This type of methodology is particularly suited to the optics of the Apogee instruments, but may be also be useful for flow cytometers with low collection angles such as jet-in-air sorters where Mie resonances make it impossible, Figure 4, to derive the particle diameter >100–150 nm from SSC alone (28). Second, using different wavelengths for scatter collection has benefits and limitations. Shorter wavelengths increase the scattering cross section of particles, while larger wavelengths produce more isotropic scattering characteristics, which makes particle sizing easier for the majority of EVs, due to Mie resonances occurring at larger diameters. Implementation of different wavelengths however may lead to practical hurdles due to collection lens chromatic aberration, system optical noise, and particle dispersion characteristics. Third, accurate calibration of flow cytometers with reference particles requires access to internal specifications of the flow cytometer, in particular the geometry of the collection optics. In cases where such proprietary component information from the manufacturer is not available, we have demonstrated here a method to determine a sufficiently precise collection angle through numerical fitting of simulated results with measured reference bead data. Finally, upon obtaining a collection half-angle of the instrument, we have demonstrated an example of determining the EV diameter distribution in absolute units (nanometers) from flow cytometer data.

By developing further understanding and controls for light scatter detection methods, especially coupled with similar ongoing advances in fluorescence detection, improved standardization of reported EV data, and therefore reproducibility of studies can be achieved. It is important that these techniques are utilized by the field and that further validation studies, which have already shown improvement in standardization and still have areas to improve take place (25). Ultimately, the development and utilization of these standardization techniques will provide a method of reproducing and understanding published data, that is currently lacking, in a field that is rapidly heading toward the development of novel diagnostics, prognostics, theranostics, and therapeutics.

## ACKNOWLEDGMENTS

The authors would like to thank Michael Ward, PhD, and Wesley Smith from ThermoFisher Scientific and Edwin van der Pol, PhD, from Amsterdam Medical Centre for useful discussions. We would also like to thank John P. Nolan, PhD, for constructive criticism of the manuscript.

## FUNDING

JAW is an International Society for Advancement of Cytometry (ISAC) Marylou Ingram Scholar 2019–2023. This work was supported by University of Southampton, Faculty of Medicine, Doctoral Training Award scheme, Higher Education Innovation Fund, European Association of Cardiothoracic Anaesthesiology, the U.S. National Institutes of Health, National Cancer Institute, 1ZIA-BC011502, and the Intramural

Research Program of the National Institutes of Health (NIH), National Cancer Institute, and Center for Cancer Research.

## CONFLICT OF INTERESTS

JCJ and JAW are inventors on patents and patent applications related to EV analysis. NCI holds a collaborative research and development agreement (CRADA) with Beckman Coulter.

## LITERATURE CITED

- van der Pol E, Boing AN, Harrison P, Sturk A, Nieuwland R. Classification, functions, and clinical relevance of extracellular vesicles. *Pharmacol Rev* 2012;64(3):676–705. <https://doi.org/10.1124/pr.112.005983>.
- Chernyshev VS, Rachamadugu R, Tseng YH, Belnap DM, Jia Y, Branch KJ, Butterfield AE, Pease LF, Bernard PS, Sklair M. Size and shape characterization of hydrated and desiccated exosomes. *Anal Bioanal Chem* 2015;407(12):3285–3301. <https://doi.org/10.1007/s00216-015-8535-3>.
- Yuana Y, Koning RJ, Kuil ME, Rensen PCN, Koster AJ, Bertina RM, Osanto S. Cryo-electron microscopy of extracellular vesicles in fresh plasma. *J Extracell Vesicles* 2013;2. <https://doi.org/10.3402/jev.v210.21494>.
- Valkonen S, Pol vE, Böing A, et al. Biological reference materials for extracellular vesicle studies. *Eur J Pharm Sci* 2017;98:4–16.
- Nielsen MH, Beck-Nielsen H, Andersen MN, Handberg A. A flow cytometric method for characterization of circulating cell-derived microparticles in plasma. *J Extracell Vesicles*. 2014;3. <https://doi.org/10.3402/jev.v3.20795>.
- Rousseau M, Belleannee C, Ducheze AC, Cloutier N, Levesque T, Jacques F, Perron J, Nigrovic PA, Dieude M, Hebert MJ, et al. Detection and quantification of microparticles from different cellular lineages using flow cytometry. Evaluation of the impact of secreted phospholipase A2 on microparticle assessment. *PLoS One* 2015;10(1):e0116812. <https://doi.org/10.1371/journal.pone.0116812>.
- Robert S, Poncelet P, Lacroix R, et al. Standardization of platelet-derived microparticle counting using calibrated beads and a Cyomics FC500 routine flow cytometer: A first step towards multicenter studies? *J Thromb Haemost* 2009;7(1):190–197. <https://doi.org/10.1111/j.1538-7836.2008.03200.x>.
- Jayachandran M, Litwiller RD, Owen WG, Heit JA, Behrenbeck T, Mulvagh SL, Araoz PA, Budoff MJ, Harman SM, Miller VM. Characterization of blood borne microparticles as markers of premature coronary calcification in newly menopausal women. *Am J Physiol Heart Circ Physiol* 2008;295(3):H931–H938. <https://doi.org/10.1152/ajpheart.00193.2008>.
- van der Pol E, van Gemert MJ, Sturk A, et al. Single vs. swarm detection of microparticles and exosomes by flow cytometry. *J Thromb Haemost* 2012;10(5):919–930. <https://doi.org/10.1111/j.1538-7836.2012.04683.x>.
- Mie G. Beiträge zur Optik trüber Medien, speziell kolloidaler Metallösungen. *Ann Phys* 1908;330(3):377–445. <https://doi.org/10.1002/andp.19083300302>.
- C. M. MATLAB functions for Mie scattering and absorption. 2002-11. Available from [http://www.atmo.arizona.edu/students/courselinks/spring09/atmo656b/maetzler\\_mie\\_v2.pdf](http://www.atmo.arizona.edu/students/courselinks/spring09/atmo656b/maetzler_mie_v2.pdf).
- Bohren CF, Huffman DR. *Absorption and Scattering of Light by Small Particles*. Chichester: Wiley, 1983.
- van der Pol E, Coumans FA, Sturk A, Nieuwland R, van Leeuwen T. Refractive index determination of nanoparticles in suspension using nanoparticle tracking analysis. *Nano Lett* 2014;14(11):6195–6201.
- Fattacioli J, Baudry J, Emerard JD, et al. Size and fluorescence measurements of individual droplets by flow cytometry. *Soft Matter* 2009;5(11):2232–2238.
- Beuthan J, Minet O, Helfmann J, Herrig M, Müller G. The spatial variation of the refractive index in biological cells. *Phys Med Biol* 1996;41(3):369–382.
- Gardiner C, Shaw M, Hole P, Smith J, Tannetta D, Redman CW, Sargent IL. Measurement of refractive index by nanoparticle tracking analysis reveals heterogeneity in extracellular vesicles. *J Extracell Vesicles* 2014;3:25361. <https://doi.org/10.3402/jev.v3.25361>.
- Valkonen S, van der Pol E, Boing A, et al. Biological reference materials for extracellular vesicle studies. *Eur J Pharm Sci* 2016.
- van Manen HJ, Verkuijlen P, Wittendorp P, Subramaniam V, van den Berg TK, Roos D, Otto C. Refractive index sensing of green fluorescent proteins in living cells using fluorescence lifetime imaging microscopy. *Biophys J* 2008;94(8):L67–L69. <https://doi.org/10.1529/biophysj.107.127837>.
- Foladori P, Quaranta A, Ziglio G. Use of silica microspheres having refractive index similar to bacteria for conversion of flow cytometric forward light scatter into biolume. *Water Res* 2008;42(14):3757–3766. <https://doi.org/10.1016/j.watres.2008.06.026>.
- Polyanskiy MN. Refractive index database. Available from: <https://refractiveindex.info>
- Stoner SA, Duggan E, Condello D, Guerrero A, Turk JR, Narayanan PK, Nolan JP. High sensitivity flow cytometry of membrane vesicles. *Cytomet Part A: J Int Soc Anal Cytol* 2016;89(2):196–206. <https://doi.org/10.1002/cyto.a.22787>.
- van der Vlist EJ, Nolte-t Hoen EN, Stoovogel W, et al. Fluorescent labeling of nano-sized vesicles released by cells and subsequent quantitative and qualitative analysis by high-resolution flow cytometry. *Nat Protoc* 2012;7(7):1311–1326.
- Wiklander OPB, Bostancioğlu RB, Welsh JA, et al. Systematic methodological evaluation of a multiplex bead-based flow Cytometry assay for detection of extracellular vesicle surface signatures. *Frontiers in immunology* 2018;9:1326. <https://doi.org/10.3389/fimmu.2018.01326>.

24. Morales-Kastresana A, Musich TA, Welsh JA, et al. High Fidelity detection and sorting of Nanoscale vesicles in viral disease and cancer. *J Extracell Vesi* 2019;8. <https://doi.org/10.1080/20013078.2019.1597603>.
25. van der Pol E, Sturk A, van Leeuwen T, et al. Standardization of extracellular vesicle measurements by flow cytometry through vesicle diameter approximation. *J Thromb Haemost* 2018;16(6):1236–1245. <https://doi.org/10.1111/jth.14009>.
26. van der Pol E, Coumans FA, Grootemaat AE, et al. Particle size distribution of exosomes and microvesicles determined by transmission electron microscopy, flow cytometry, nanoparticle tracking analysis, and resistive pulse sensing. *J Thromb Haemost* 2014;12(7):1182–1192. <https://doi.org/10.1111/jth.12602>.
27. Varga Z, van der Pol E, Palmai M, et al. Hollow organosilica beads as reference particles for optical detection of extracellular vesicles. *J Thromb Haemost* 2018;16: 1646–1655.
28. van der Pol E, de Rond L, Coumans FAW, Gool EL, Böing AN, Sturk A, Nieuwland R, van Leeuwen TG. Absolute sizing and label-free identification of extracellular vesicles by flow cytometry. *Nanomedicine* 2018;14(3):801–810. <https://doi.org/10.1016/j.nano.2017.12.012>.